Superposed flow between two discs contrarotating at differential speeds

X. Gan, M. Kilic* and J. M. Owen
School of Mechanical Engineering, University of Bath, Claverton Down, Bath, UK

This paper describes a combined computational and experimental study of the flow between two contrarotating discs for $-1 \leq \Gamma \leq 0$ (where Γ is the ratio of the speed of the slower disc to that of the faster one) for the case where there is a superposed radial outflow of air. The computations were conducted using an elliptic solver and a low-Reynolds-number k–ε turbulence model, and velocity measurements were made using a laser-Doppler anemometry system. Two basic flow structures can occur: Batchelor-type flow, where there are separate boundary layers on each disc with a rotating core of fluid between, and Stewartson-type flow, where there is virtually no core rotation. The main effect of a superposed flow is to reduce the core rotation and to promote the transition from Batchelor-type flow to Stewartson-type flow. For most of the results, there is good agreement between the computed and measured velocities. Computed moment coefficients show that, for $\Gamma = -1$, superposed flow has little effect on C_m: an accepted correlation of C_m for a free disc should provide a useful estimate for design purposes.

Keywords: contrarotating discs; rotating discs; rotating flow

1. Introduction

One of the practical applications for contrarotating discs is in gas-turbine aeroengines where, in future generations of ultra-high-bypass-ratio engines, contrarotating turbines may be used to drive contrarotating fans. This has the advantage of eliminating a row of stator nozzles, thereby reducing the size and weight of the engine. The designer of the internal-air systems uses a superposed radial flow of air to cool the turbine discs and to remove the heat generated by windage, and there is comparatively little information on the flow in contrarotating disc systems.

A schematic diagram of the flow structure is shown in Figure 1. The flow is radially outwards in the boundary layers on the discs and radially inward between the boundary layers. The precise flow structure depends on Γ, where Γ is the ratio of the angular speed of the slower disc, Ω_2, to that of the faster one, Ω_1, on the rotational Reynolds number, $\mathrm{Re}_\phi = \rho\Omega_1 b^2/\mu$, and on the nondimensional flowrate, $C_w = \dot{m}/\mu b$. $\Gamma = 0$ corresponds to the rotor-stator case, considered in detail by Owen and Rogers (1989); $\Gamma = -1$ corresponds to antisymmetrical contrarotation.

Two different flow structures have been predicted for $-1 \leq \Gamma \leq 0$. Batchelor (1951), from consideration of the laminar flow between two infinite discs, deduced that for $\Gamma = 0$, the rotor-stator case, there would be radial outflow in a boundary layer on the rotating disc, inflow in a boundary layer on the stationary one, and a core of rotating fluid between. For $\Gamma = -1$, he predicted radial outflow in boundary layers on both discs and radial inflow in a thin shear layer in the midplane ($z/s = \frac{1}{2}$), with a rotating core on either side of the shear layer. Stewartson (1953) predicted different flow structures: for $\Gamma = 0$, there would be no boundary layer on the stator and no rotation outside the boundary layer on the rotor; for $\Gamma = -1$, there would be no contrarotating cores of fluid, and radial inflow would occur in the single, nonrotating core between the boundary layers on the discs. It is now apparent that there are no unique solutions for the flow between infinite discs, and Batchelor's and Stewartson's solutions are both possible; the interested reader is referred to the review by Zandbergen and Dijkstra (1987) for a detailed account.

Dijkstra and van Heijst (1983) carried out a comprehensive computational and experimental study for laminar flow for $-0.825 \leq \Gamma \leq 0$ and values of Re_ϕ up to 2.04×10^5. For the experiments, they used a rig, with discs around 1 m diameter spaced 35 mm apart ($G = 0.07$), filled with water or with a mixture of water and glycerol. For $\Gamma = 0$, they found

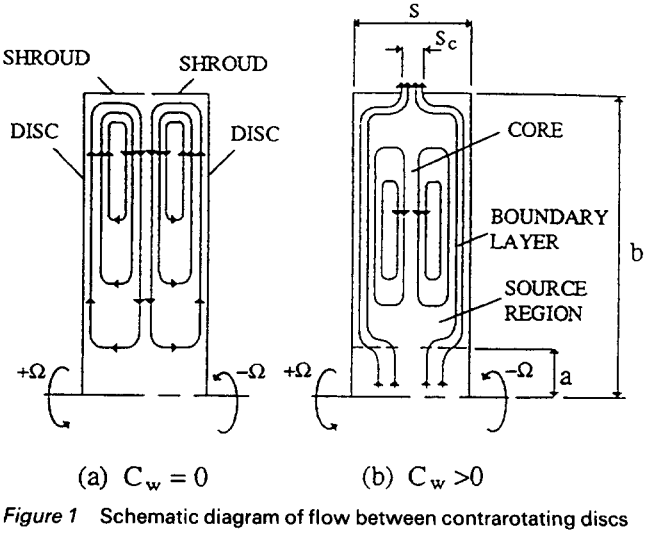

Figure 1 Schematic diagram of flow between contrarotating discs

* Currently at Uludağ Universitesi, Mühendislik-Mimarlik Fakultesi, Makina Bolumu, Bursa, Turkey.

Address reprint requests to Professor Owen at the School of Mechanical Engineering, University of Bath, Claverton Down, Bath BA2 7AY, UK.

Received 12 November 1993; accepted 3 June 1994

Batchelor-type flow, with boundary layers on the rotor and stator and a rotating core between. For $-0.825 \leq \Gamma \leq -0.15$, they found a two-cell structure with an outer cell in which Batchelor-type flow occurred and an inner one with Stewartson-type flow; the two cells were separated by a streamline that stagnated on the slower disc. No reliable computational or experimental data were obtained for $-1 \leq \Gamma \leq -0.825$, where wavy instabilities were observed.

Graber et al. (1987) reported extensive experimental measurements for enclosed rotating-disc systems with a stationary shroud. Their pressurized rig consisted of two discs of 0.534 m diameter that could be rotated independently in either direction at speeds up to 3,500 rev/min. For their tests, $G = 0.328$, and the ratio of inner and outer radii was $a/b = 0.248$. They made the measurements for $\mathrm{Re}_\phi = 4 \times 10^6$, 8×10^6, and 1.6×10^7 and for $\Gamma = -1$, 0, and 1 with superposed flow rates of air in the range $-0.14 \leq \lambda_T \leq 0.14$, where $\lambda_T (= C_w \mathrm{Re}_\phi^{-0.8})$ is the turbulent flow parameter, and the negative sign indicates radial inflow. They observed that the moment coefficient, C_m, for $\Gamma = -1$ was approximately twice that for $\Gamma = 0$ (the rotor-stator case); the insertion of a stationary disc between the contrarotating ones reduced the moment coefficient to the same level as that of the rotor-stator system.

Morse (1988) used an elliptic solver, featuring a modified version of the Launder–Sharma (1974) low-Reynolds-number k–ε (LR k–ε) turbulence model, to compute the axisymmetric flow inside rotating cavities; details of these LR k–ε models are given in the appendix. Morse initially used a modified version of the near-wall damping function, f_μ, proposed by Launder and Sharma, but in his later work (Morse 1991a, 1991b) he employed a version of f_μ similar to that proposed by Nagano and Hishida (1987). Using these modified LR k–ε models, Morse was able to make accurate predictions of the flow in a number of rotating-disc systems at rotational Reynolds numbers as high as $\mathrm{Re}_\phi = 10^7$, typical of the values found in engines. Of particular relevance to the work considered here are the computations of Morse (1991a) for flow between contrarotating discs for $G = 0.1$, $10^5 \leq \mathrm{Re}_\phi \leq 10^7$, and $-1 \leq \Gamma \leq 0$; like Graber et al. (1987), Morse considered the case where the peripheral shroud was stationary. For the turbulent contrarotating case, Morse found that there was a stagnation ring on the slower disc where the radial inflow and outflow meet, which is consistent with the findings of Dijkstra and van Heijst for laminar flow.

Gan et al. (1993) conducted a combined computational and experimental study of the flow between contrarotating discs with $G = 0.12$, $10^5 \leq \mathrm{Re}_\phi \leq 1.25 \times 10^6$, $0 \leq C_w \leq 9{,}280$, and $\Gamma = -1$. For the experiments (using the rig described in Section 3), the velocities were measured by laser-Doppler anemometry (LDA). For the computations, a multigrid elliptic solver was used (see Section 2) together with a variant of Morse's (1991a, 1991b) LR k–ε turbulence model. Computations using the turbulence model produced the Stewartson-type flow structure in contrast with the computations for laminar flow (where all turbulent terms were set to zero), which produced the Batchelor-type structure. The laminar flow structure, while providing a valid solution of the Navier–Stokes equations, is intrinsically unstable, and no experimental evidence was found for its physical existence, even for rotational Reynolds-number as low as $x^2\mathrm{Re}_\phi = 2.2 \times 10^4$. Although the turbulence model exhibited premature transition from laminar to turbulent flow in the boundary layers on the discs, the agreement between the computed and measured velocities was mainly good over a wide range of flow rates and rotational speeds.

A combined computational and experimental study of the transition from turbulent Batchelor-type flow at $\Gamma = 0$ to Stewartson-type flow at $\Gamma = -1$ was investigated by Kilic et al. (1994) for the case of $C_w = 0$. The turbulent computations showed that, as found by Dijkstra and van Heijst for laminar flow, at intermediate values of Γ a two-cell structure is formed with Batchelor-type flow in the outer cell and Stewartson-type flow in the inner one, as shown in Figures 2 and 3 for $\mathrm{Re}_\phi = 1.25 \times 10^6$. For $\Gamma = 0$ and -0.2, the single-cell Batchelor-type flow can be seen in Figure 2, and Figure 3 shows that there is zero radial velocity in the rotating core between the boundary layers. For $\Gamma = -1$, the single-cell Stewartson-type flow occurs with radial inflow in the (virtually) nonrotating core. For $-0.8 \leq \Gamma \leq -0.4$, Figure 2 shows a two-cell structure with a stagnation point on the slower disc at $x = x_{st}$; the radius of the stagnation point increases as Γ decreases. For this two-cell structure, Figure 3 confirms that Batchelor-type flow, with a rotating core, occurs for $x > x_{st}$, and

Notation

a	Inner radius of disc
b	Outer radius of disc
C_m	Moment coefficient for one side of the disc, $(= M/\frac{1}{2}\rho\Omega^2 b^5)$
C_w	Nondimensional flow rate $(= \dot{m}/\mu b)$
f_μ	Near-wall damping function in turbulence model
G	Gap ratio $(= s/b)$
G_c	Shroud-clearance ratio $(= s_c/b)$
k	Turbulent kinetic energy
$\dot{m}$	Mass flow rate
M	Moment on one side of disc 1
r	Radial coordinate
R_T	Turbulent Reynolds number $(= \rho k^2/\varepsilon\mu)$
Re_ϕ	Rotational Reynolds number $(= \rho\Omega_1 b^2/\mu)$
s	Axial gap between discs
s_c	Axial clearance between shrouds
u_τ	Friction velocity $(= \sqrt{\tau_w/\rho})$
V_r, V_ϕ, V_z	Velocity components referred to stationary cylindrical coordinates (r, ϕ, z)
x	Nondimensional radius $(= r/b)$
y	Normal distance from wall
$y+$	Nondimensional near-wall distance $(= \rho u_\tau y/\mu)$
z	Axial coordinate measured from disc 1

Greek symbols

Γ	Ratio of angular speeds of contrarotating discs $(= \Omega_2/\Omega_1)$
ε	Rate of dissipation of turbulent kinetic energy
λ_T	Turbulent flow parameter $(= C_w \mathrm{Re}_\phi^{-0.8})$
μ	Dynamic viscosity
ρ	Density
τ_w	Wall shear stress
Ω	Angular speed of disc

Subscripts

1, 2	Faster (left-hand-side) disc, slower (right-hand-side) disc

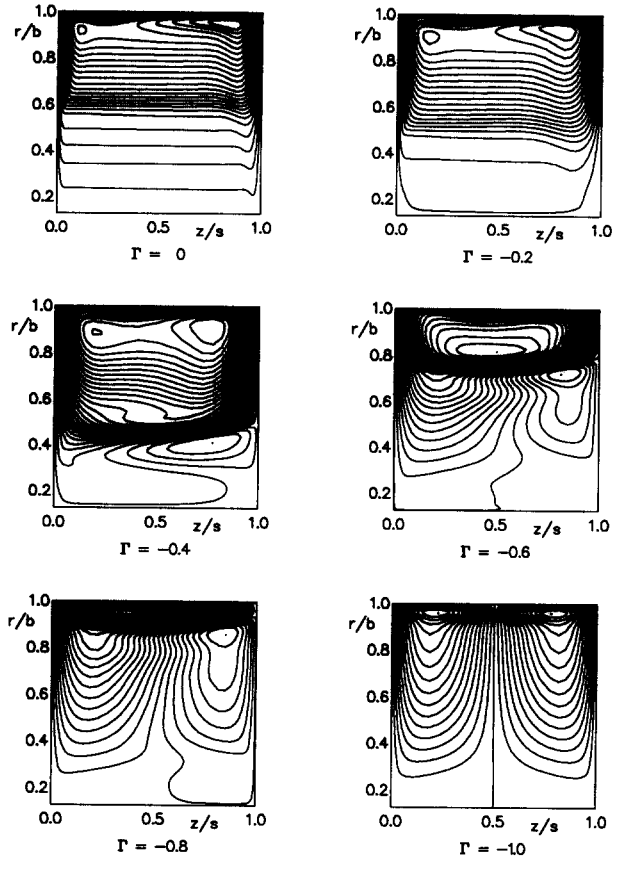

Figure 2 Computed streamlines for $Re_\phi = 1.25 \times 10^6$, $C_w = 0$

Stewartson-type flow, with a nonrotating core, occurs for $x < x_{st}$. In the main, these computed velocities were in very good agreement with the measurements.

It is the objective of this paper to present, for the first time, the results of a combined computational and experimental study of the effect of a superposed flow on the turbulent flow structure between rotating discs for $-1 \leq \Gamma \leq 0$. Sections 2 and 3 outline the computational method and the experimental apparatus, respectively, and the comparison between computations and measurements is presented in Section 4.

2. Computational method

The Reynolds-averaged Navier–Stokes equations for steady, axisymmetric, incompressible flow were solved in conjunction with an LR k–ε turbulence model. The code used was a modified version of the elliptic multigrid solver described by Vaughan et al. (1989), where finite-volume equations were obtained using the control-volume approach of Patankar (1980) together with the SIMPLEC pressure-correction algorithm proposed by van Doormaal and Raithby (1984). The multigrid method was developed by Vaughan et al. for turbulent flow from the full-approximation scheme employed by Lonsdale (1988) to solve the Navier–Stokes equations for laminar flow between corotating discs; a three-level V-cycle was used for the computations discussed below. Details of the conservation equations and the turbulence model are given in the appendix.

Gan et al. (1993) used the above code, together with a variant of the Morse (1991a, 1991b) LR k–ε turbulence model, to compute the flow between contrarotating discs for $\Gamma = -1$. Kilic (1993) used both the Morse turbulence model and the original Launder and Sharma (1974) model to compute the flow for $-1 \leq \Gamma \leq 0$. As can be seen from the appendix, the Morse model uses a near-wall damping function, f_μ, based on the nondimensional distance, y^+, from the nearest wall. This function can cause difficulties in corner regions, where two boundary layers interact, resulting in convergence problems for the multigrid solver at high values of Re_ϕ, and the results presented in this paper were obtained using only the Launder–Sharma turbulence model. (Computed velocity profiles produced using either of these models were, in the main, in good agreement with most of the measured values.)

The computational geometry was based on that of the rig described in Section 3, where the radius ratio was $a/b = 0.13$ and the gap ratio was $G = 0.12$. For the solid boundaries ($z = 0$, $z = s$, $r = a$, $r = b$), no-slip conditions were used. For the axial clearance, s_c, between the shrouds attached to the discs at $r = b$, it was assumed that the flow left radially with linear swirl:

$$V_r = \frac{\dot{m}}{2\pi\rho b s_c}$$

$$V_\phi = \frac{1}{2}\Omega_1 b\left((1+\Gamma) + (1-\Gamma)\frac{s-2z}{s_c}\right)$$

$$V_z = 0$$

The air was assumed to enter the cavity radially without swirl at $r = a$, so that:

$$V_r = \frac{\dot{m}}{2\pi\rho a s}$$

$$V_\phi = 0$$

$$V_z = 0$$

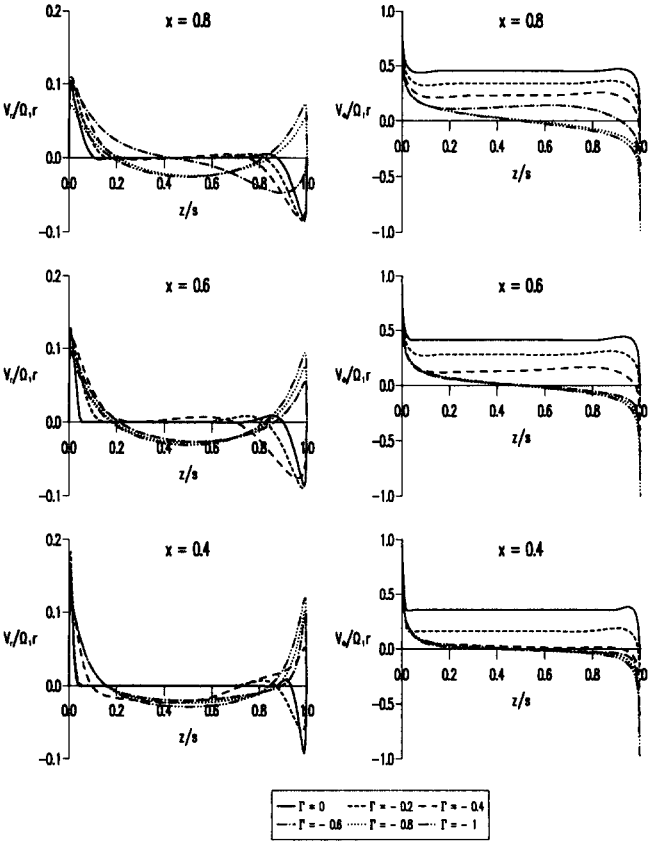

Figure 3 Computed velocity profiles for $Re_\phi = 1.25 \times 10^6$, $C_w = 0$

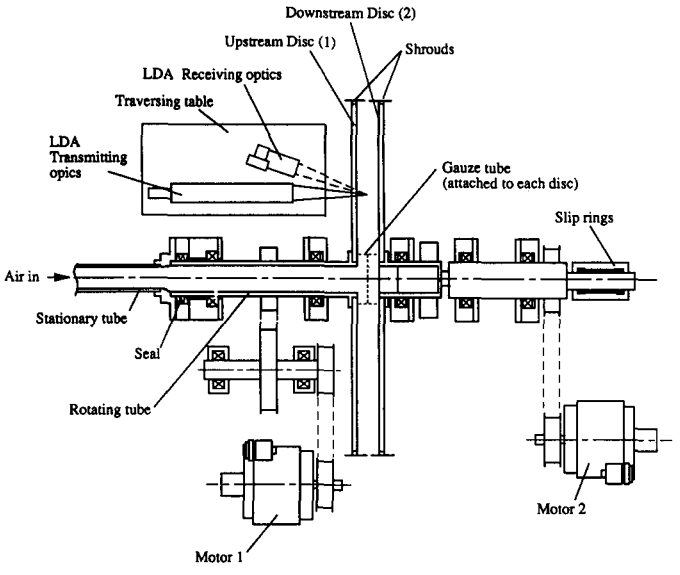

Figure 4 Schematic layout of rotating-disc rig and LDA system

The assumed inlet conditions did not precisely match those in the experiment, where flow was admitted axially through a central hole in disc 1 and entered the cavity between the two discs radially through porous tubes. Some computations were carried out using other inlet conditions, but, away from the inlet, the effect on the computed velocity distribution was relatively small.

Tests were conducted using a number of convergence criteria including RMS^{Φ}, the root-mean-square change in the computed variables from one iteration to the next, the total absolute value of the residuals, and R^{Φ}_{max}, the maximum value of the residuals for each variable. Converged solutions were achieved for $RMS^{\Phi} \approx 10^{-4}$ and $R^{\Phi}_{max} \approx 10^{-5}$ for all variables. Grid-dependency tests were also conducted with up to 91 × 115 (axial x radial) nodes, and it was found that a grid with 67 × 67 nodes (contracted to the boundaries) gave sensibly grid-independent results. (Morse (1991b) chose grid-expansion factors that ensured that the grid point adjacent to a wall was located at a nondimensional distance of $y^+ < 0.5$; this criterion was used for the computations presented here.)

The computations were conducted on one i860 node of a 16-node Meiko parallel-computing facility. The time to achieve a converged solution depended on Γ, Re_ϕ, and C_w, but typical times for 91 × 115 nodes ranged from one to two hours.

Further details of the computational method are given by Kilic (1993).

3. Experimental apparatus

A schematic layout of the rotating-disc rig and LDA system is shown in Figure 4.

The discs, which were 762 mm in diameter, were independently rotated at up to 1,500 rev/min by two thyristor-controlled electric motors. A peripheral shroud was attached to each disc, the axial clearance between the shrouds was less than 4 mm, and the axial spacing between the discs produced a gap ratio of $G = 0.12$. Air was supplied through a central hole in disc 1, and it entered the cavity between the two discs via a porous tube, 100 mm in diameter, attached to the center of each disc. This inlet arrangement was intended to create a uniform radial source, but, as discussed below, the actual flow was nonuniform. The flow rate of the air was measured, with an uncertainty of ±3 percent, using an orifice plate in a stationary pipe upstream of the rig. Seals between the rotating and stationary pipes reduced the leakage to a negligible level.

Disc 2 was made from transparent polycarbonate, and a single-component TSI laser-Doppler anemometry (LDA) system was used to measure the radial and tangential components of velocity. The LDA system was arranged in a back-scatter mode, and a TSI IFA 750 burst correlator was used to measure the Doppler frequency created by scattering from micron-sized oil particles seeded into the air. With the optical "probe-volume" of the LDA system focused inside the polycarbonate disc, the tangential component of velocity of the disc could be measured: the difference between this and the independently measured angular speed of the disc was typically less than 0.5 percent of the speed.

4. Comparison between computations and measurements

4.1. Velocity profiles

Figures 5 to 9 show comparisons between the computed and measured nondimensional radial and tangential components of velocity ($V_r/\Omega_1 r$ and $V_\phi/\Omega_1 r$) for $Re_\phi = 1.25 \times 10^6$, $C_w = 6{,}100$, and $\Gamma = 0$, -0.4, -0.6, -0.8, and -1, respectively. These should be compared with the computed velocities for the equivalent cases with $C_w = 0$ in Figure 3.

For $\Gamma = 0$, Figure 5 shows that a superposed flow reduces both the core rotation and the radial inflow on the stationary disc. For $x = 0.6$, the computations show that the core rotation and the radial inflow are negligible, although the measured velocities still show weak rotation and inflow at this radius.

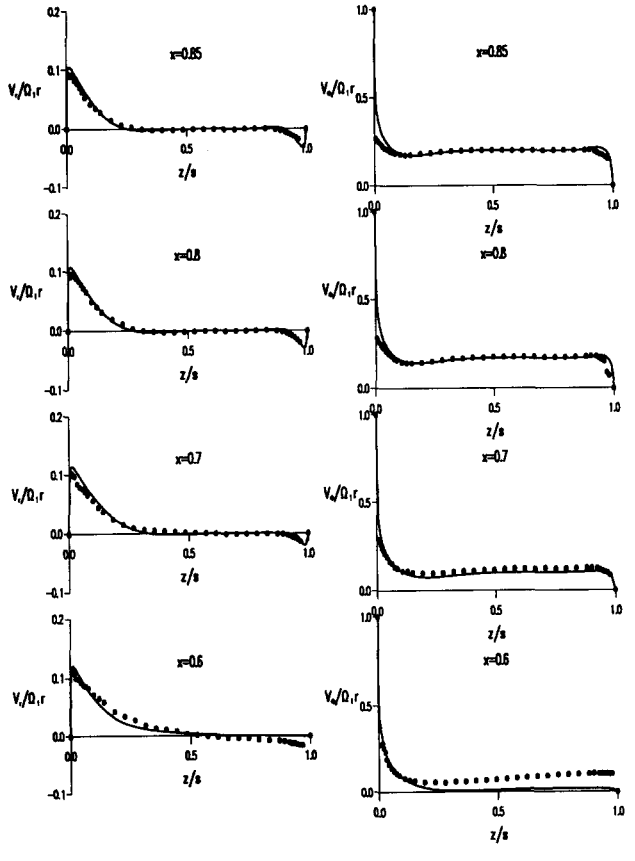

Figure 5 Computed and measured velocity profiles for $Re_\phi = 1.25 \times 10^6$, $\Gamma = 0$, $C_w = 6{,}100$

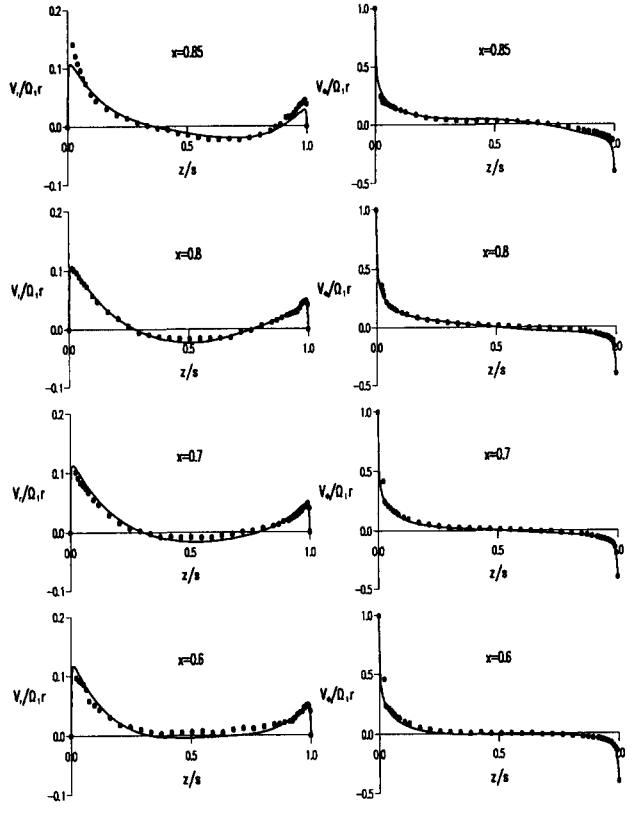

Figure 6 Computed and measured velocity profiles for $Re_\phi = 1.25 \times 10^6$, $\Gamma = -0.4$, $C_w = 6{,}100$

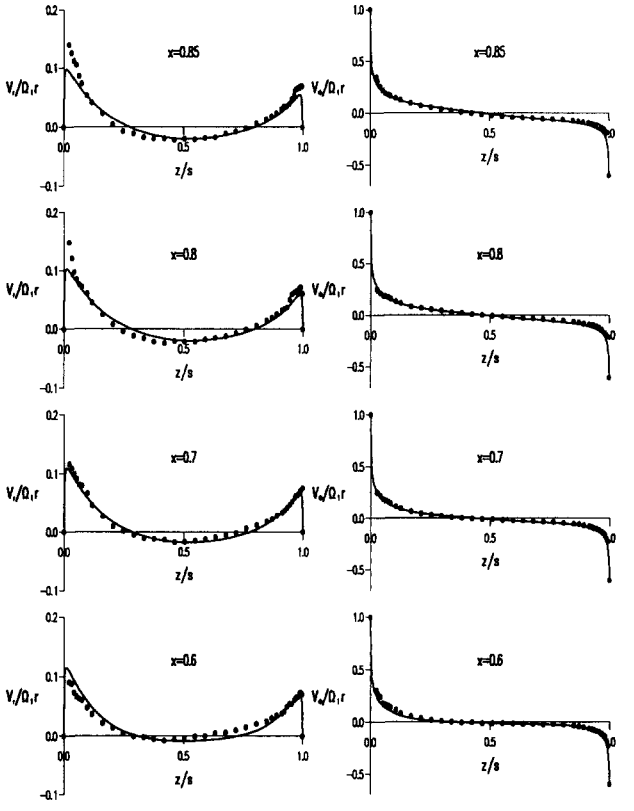

Figure 7 Computed and measured velocity profiles for $Re_\phi = 1.25 \times 10^6$, $\Gamma = -0.6$, $C_w = 6{,}100$

For $C_w = 0$, Figure 3 shows that $V_\phi/\Omega_1 r \approx 0.4$ in the core for $\Gamma = 0$.

For $\Gamma = -0.4$, Figure 6 shows no evidence of Batchelor-type flow: there is radial outflow in boundary layers on both discs with radial inflow in the (virtually) nonrotating core between the boundary layers. This is in contrast to the case with $C_w = 0$, where Figure 3 shows Batchelor-type flow for $x \geq 0.6$ with radial inflow on the slower disc and core rotation between the boundary layers.

For $\Gamma = -0.6$, -0.8, and -1, Figures 7, 8, and 9 show that Stewartson-type flow occurs everywhere, with radial outflow on both discs and inflow in the core. Even for $C_w = 0$, Figure 3 shows that Stewartson-type flow occurs at these values of Γ.

With few exceptions, the computations and measurements are in very good agreement. Even when $C_w = 0$, Batchelor-type flow is converted to Stewartson-type flow as Γ is reduced from 0 to -1. For $C_w > 0$, the transition from Batchelor-type flow to Stewartson-type flow occurs at larger values of Γ than for $C_w = 0$.

In an engine, the rotational Reynolds number is of the order of 10^7, which is considerably higher than that achievable on the existing rig. It is useful to relate the superposed flow rate to the rotational speed using the turbulent flow parameter, $\lambda_T = C_w Re_\phi^{-0.8}$ (see Owen and Rogers 1989). A value of $\lambda_T = 0.22$ corresponds to the flow rate entrained by a free disc (that is, a disc rotating in an infinite environment), and in engines, λ_T is usually significantly less than this. In experiments, it is appropriate to keep λ_T, rather than C_w, in the engine range, even if a representative value of Re_ϕ cannot be achieved.

The effect of λ_T on the velocity distribution, for $\Gamma = -1$ and $Re_\phi \approx 4 \times 10^5$, is shown in Figures 10 to 13. In Figure 10, where $\lambda_T = 0.086$, the velocity distribution for $x \geq 0.8$ is similar to that in Figure 9, for $Re_\phi = 1.25 \times 10^6$, where $\lambda_T = 0.081$.

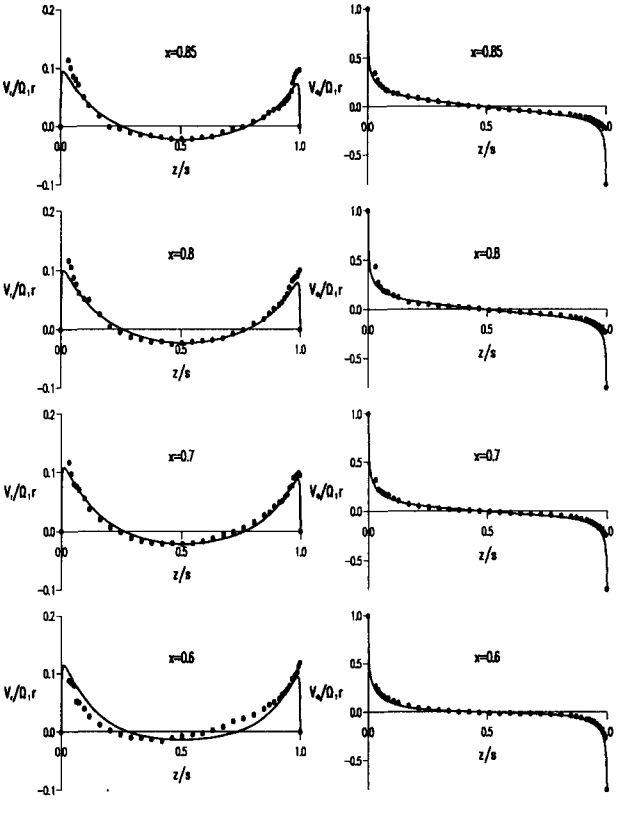

Figure 8 Computed and measured velocity profiles for $Re_\phi = 1.25 \times 10^6$, $\Gamma = -0.8$, $C_w = 6{,}100$

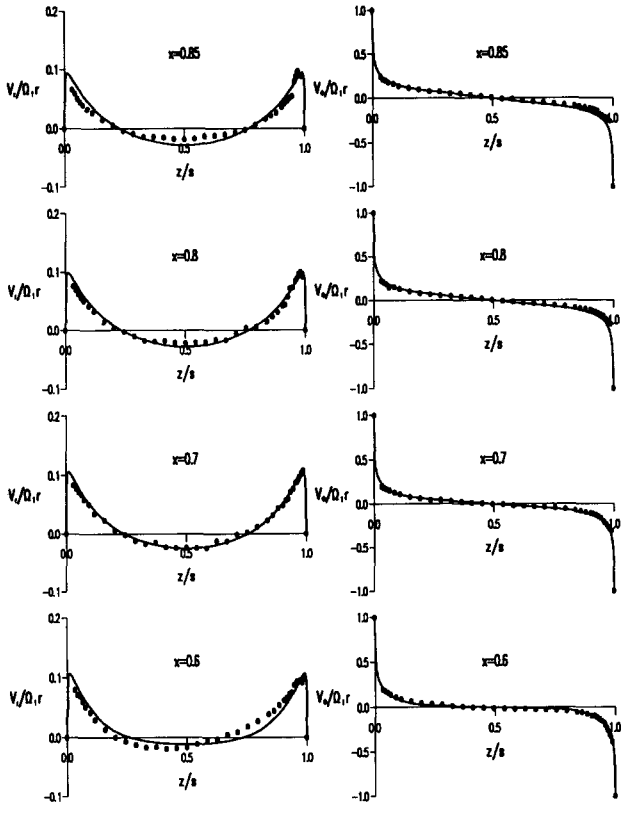

Figure 9 Computed and measured velocity profiles for $Re_\phi = 1.25 \times 10^6$, $\Gamma = -1$, $C_w = 6{,}100$, $\lambda_T = 0.0809$

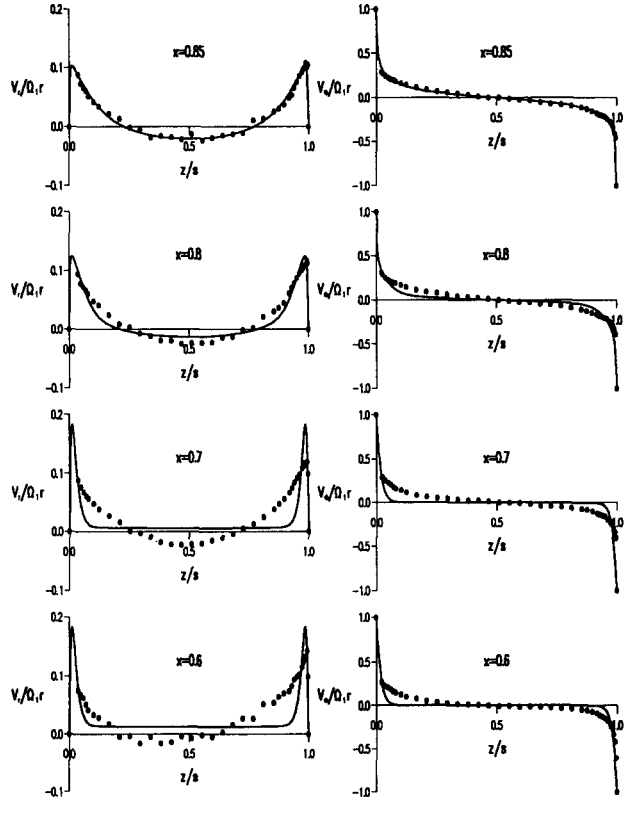

Figure 10 Computed and measured velocity profiles for $Re_\phi = 3.72 \times 10^5$, $\Gamma = -1$, $C_w = 2{,}459$, $\lambda_T = 0.0860$

For the smaller values of x, the difference between the computed and measured values in Figure 10 is attributed partly to the inlet conditions. As explained in Section 3, porous tubes were used in the experimental rig to create a uniform source at $x = 0.13$. In practice, the flow is skewed, and symmetry about the midplane is not achieved at the smaller values of x. Another difference is caused by the fact that, at this low value of Re_ϕ, the turbulence model produces laminar flow in the boundary layers for $x \leq 0.7$, whereas the measurements show that turbulent flow occurs. (In Figure 9, for $Re_\phi = 1.25 \times 10^6$, both computations and experiments show that turbulent flow occurs.)

In Figure 11, for $\lambda_T = 0.14$, both the computations and the measurements show evidence of a source region at the smaller values of x. In the source region, the superposed flow is greater than that entrained by the boundary layers on the discs, and so there is a radial outflow between the boundary layers. The entrainment for laminar flow is less than for turbulent flow, and consequently the computations overestimate the size of the source region.

Figures 12 and 13, for $\lambda_T = 0.21$ and 0.31, show that the size of the source region increases as λ_T increases. Again, the computations show laminar flow in the boundary layers at the smaller radii, but the agreement between the measured and computed velocities improves at the larger radii where the computed flow is turbulent.

4.2. Moment coefficients

The frictional moment, M, on the rotating discs was not measured for the rig described in Section 3.

For the case of the free disc and for rotor-stator systems, there have been many measurements of the moment coefficient,

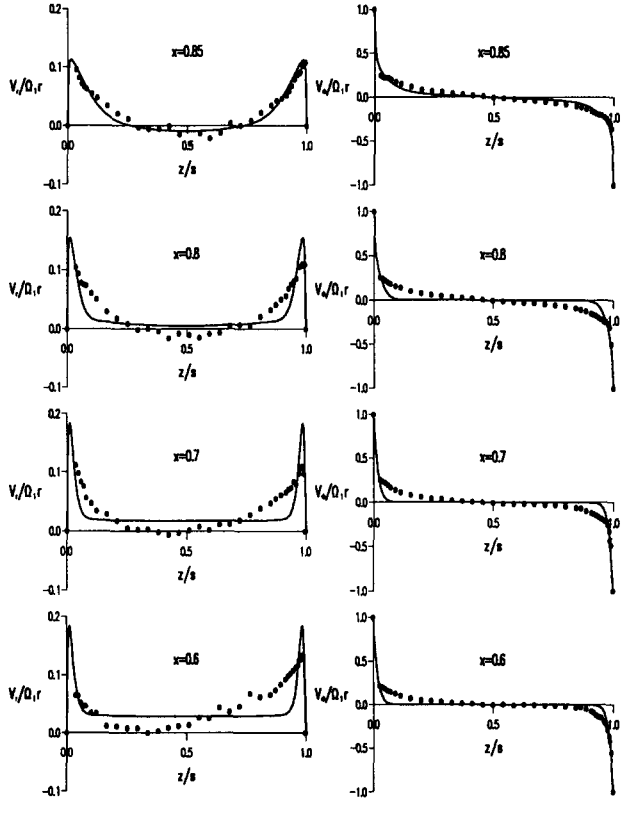

Figure 11 Computed and velocity profiles for $Re_\phi = 3.83 \times 10^5$, $\Gamma = -1$, $C_w = 4{,}061$, $\lambda_T = 0.1387$

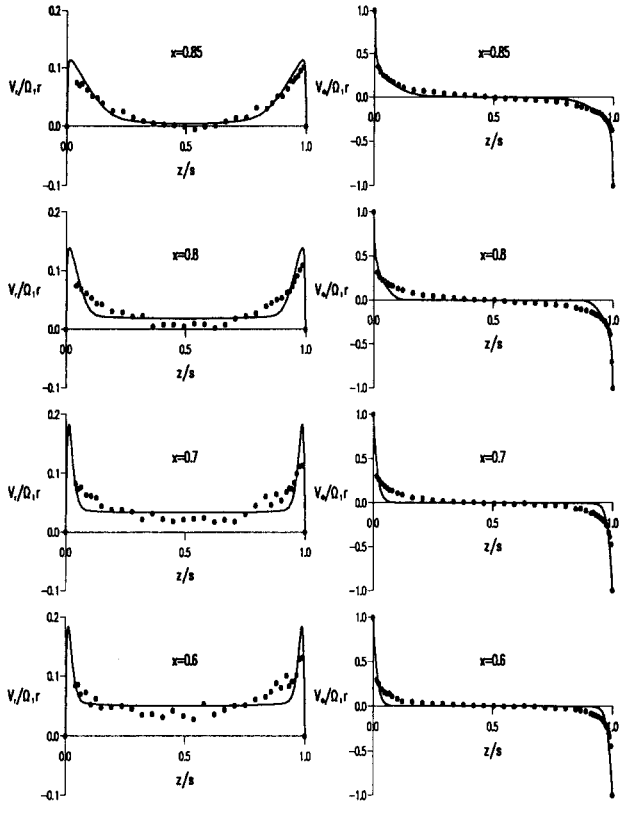

Figure 12 Computed and measured velocity profiles for $Re_\phi = 3.80 \times 10^5$, $\Gamma = -1$, $C_w = 6{,}114$, $\lambda_T = 0.2101$

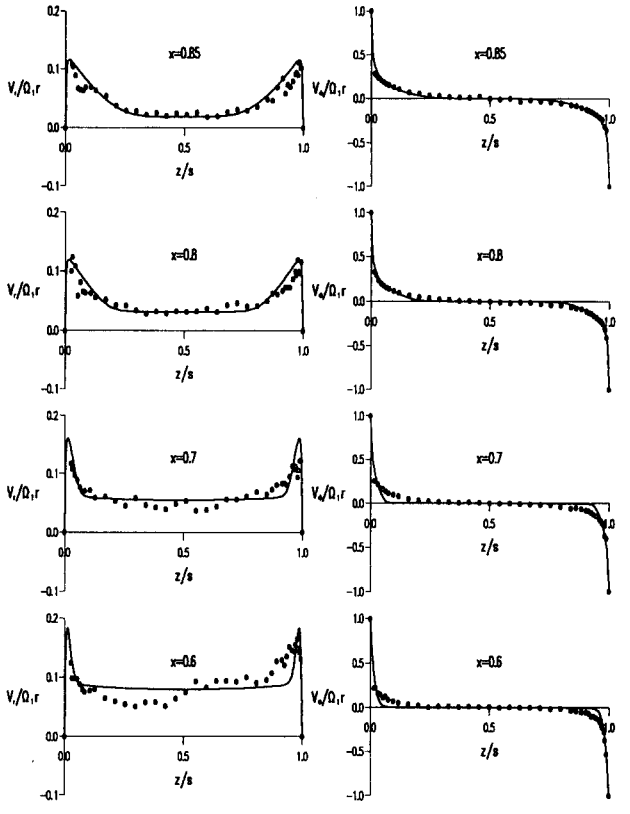

Figure 13 Computed and measured velocity profiles for $Re_\phi = 3.93 \times 10^5$, $\Gamma = -1$, $C_w = 9{,}378$, $\lambda_T = 0.3139$

C_m, as described by Owen and Rogers (1989). The most accurate equation for C_m for the turbulent free disc is that derived by Dorfman (1963), where

$$C_m = 0.491 \, (\log_{10} Re_\phi)^{-2.58} \quad (1)$$

This equation is in good agreement with the available experimental data for free discs for $7 \times 10^5 \leq Re_\phi \leq 7 \times 10^6$; transition from laminar to turbulent flow occurs for $Re_\phi \geq 3 \times 10^5$, although disc roughness or environmental disturbances can cause premature transition at lower values of Re_ϕ.

For enclosed rotor-stator systems ($\Gamma = 0$), in the absence of a superposed flow, Daily and Nece (1960) made measurements of C_m for $0.0127 \leq G \leq 0.217$ and $10^3 < Re_\phi < 10^7$. There are four flow regimes, depending on G and Re_ϕ, but for the case of turbulent flow with separate boundary layers on the rotor and stator, which is relevant to the conditions considered here, their empirical correlation is

$$C_m = 0.051 \, G^{0.1} \, Re_\phi^{-0.2} \quad (2)$$

For contrarotating discs, for $\Gamma = -1$, $G = 0.1$, and $10^6 < Re_\phi < 10^7$, Morse (1991a) correlated his computations for turbulent flow by

$$C_m = 0.0319 \, Re_\phi^{-0.1375} \quad (3)$$

Morse's computations, like the experimental results of Graber et al. (1987), showed that C_m for $\Gamma = -1$ was approximately double that for $\Gamma = 0$. It should be noted that both Morse and Graber et al. considered the case where the peripheral shroud was stationary.

The elliptic solver described in Section 2 was used to compute C_m for the free disc, for rotor-stator systems, and for contrarotating discs. For the free-disc computations, the transition from laminar to turbulent flow started at $Re_\phi \approx 1.8 \times 10^5$; for smaller values of Re_ϕ, the computations were in good agreement with Cochran's (1934) exact solutions of the Navier–Stokes equations; for $Re_\phi > 1.8 \times 10^5$, the computations approached Dorfman's turbulent correlation (Equation 1), and for $Re_\phi > 4 \times 10^6$, the difference between the computations and this equation was less than 1 percent. The computed moment coefficients were also compared with the Daily and Nece correlations (Equation 2). For $G = 0.08$ and $Re_\phi = 10^6$, the computed value of C_m was 13 percent lower than the correlations; for $G = 0.0637$ and $Re_\phi = 4.4 \times 10^6$, it was 2 percent lower.

Table 1 shows the computed values of C_m for the antisymmetrical contrarotating case, $\Gamma = -1$, for $C_w = 0$, $0.06 \leq G \leq 0.24$, and $1.25 \times 10^6 \leq Re_\phi \leq 10^7$; the geometry was based on the rig described in Section 3 (rotating shrouds and $a/b = 0.13$). Also shown for comparison are the free-disc results according to Equation 1. For $G = 0.06$, the computed values of C_m for $\Gamma = -1$ are close to the free-disc values, and

Table 1 Computed moment coefficients for $\Gamma = -1$, $1.25 \times 10^6 \leq Re_\phi \leq 10^7$ and $0.06 \leq G \leq 0.24$

	$\lvert C_M \rvert \times 10^3$				
$Re_\phi \times 10^{-6}$	$G = 0.06$	$G = 0.12$	$G = 0.18$	$G = 0.24$	Free disc
1.25	4.60	4.19	4.08	3.99	4.63
2	4.27	3.87	3.80	3.74	4.25
4	3.85	3.50	3.44	3.40	3.77
8	3.53	3.18	3.10	3.09	3.36
10	3.45	3.09	3.03	3.02	3.24

they are also within approximately 2 percent of the Morse correlation (Equation 3), which was obtained for $G = 0.1$. The computed values of C_m for $G = 0.06$ are approximately double those given by Equation 2 for the rotor-stator case, as was also observed by Graber et al.

It can be seen from Table 1 that C_m decreases as G increases from 0.06 to 0.24; for $G > 0.24$, the computed values of C_m were found to be virtually independent of G. The trend of decreasing C_m with increasing G for $\Gamma = -1$ (with rotating shrouds) is contrary to the trend of increasing C_m for $\Gamma = 0$ (with a stationary shroud), and some explanation is required. For $\Gamma = 0$, there is a core of rotating fluid between the boundary layers on the rotor and stator, and the moment on the rotor is less than that for the free-disc case. Increasing G increases the width of the *stationary* shroud, which in turn reduces the core rotation and increases the moment on the rotating disc. For $\Gamma = -1$, the sum of the moments on the discs and the *rotating* shrouds equals the rate of change of angular momentum given to the recirculating fluid; as G increases, the moment on the shroud increases and those on the discs decrease. Computations of C_m were also conducted for $\Gamma = -1$, $G = 0.12$, $1.26 \times 10^5 < \mathrm{Re}_\phi < 1.25 \times 10^6$, and $2{,}300 < C_w < 9{,}400$. Although the effect of a superposed flow was to increase C_m, the effect was small, as found experimentally by Graber et al.: increasing λ_T from zero to 0.2 (the approximate free-disc entrainment rate) only increases C_m by 6 percent. For most gas-turbine cooling systems, $\lambda_T < 0.2$, and so the effect of cooling flow rate on the disc windage is likely to be negligible: the correlation for the free disc (Equation 1) should provide a reasonable estimate for C_m.

Although, as stated above, the moment coefficients were not measured on the experimental rig, Nusselt numbers were determined during a separate series of tests. The comparison between the computed and measured Nusselt numbers will be reported elsewhere, but it is worth noting that the agreement was mainly good: the Reynolds analogy between the moment coefficients and the Nusselt numbers (see Owen and Rogers 1989) suggests that if the Nusselt numbers are accurately predicted, then the computed moment coefficients should also be accurate.

5. Conclusions

For $G = 0.12$, $\mathrm{Re}_\phi = 1.25 \times 10^6$, $C_w = 6{,}100$, and $-1 \le \Gamma \le 0$, the computed velocity distributions, obtained using the Launder and Sharma (1974) low-Reynolds-number k–ε turbulence model, are mainly in very good agreement with the experimental measurements on a purpose-built contrarotating-disc rig. The main effect of a superposed flow is to accelerate the transition from a Batchelor-type flow structure to a Stewartson-type one. Whereas Batchelor-type flow had previously been observed when $C_w = 0$ for the rotor-stator case, $\Gamma = 0$, a value of $C_w = 6{,}100$ reduced the core rotation and the radial inflow on the stationary disc. For $\Gamma \le -0.4$, there was no evidence of Batchelor-type flow, and Stewartson-type flow occurred everywhere; for $\Gamma = -0.4$, Batchelor-type flow had previously been observed for $C_w = 0$.

For $\Gamma = -1$ and $\mathrm{Re}_\phi = 4 \times 10^5$, the computations for $0.086 \le \lambda_T \le 0.31$ showed laminar flow in the boundary layers for the smaller values of x, whereas the measurements showed that the flow was turbulent. For the larger values of x, there was mainly good agreement between the measured and computed velocities. The results for $\lambda_T \ge 0.14$ showed evidence of a source region, at the smaller values of x, where the flow is radially outwards in the core between the boundary layers, and the size of the source region increases as λ_T increases.

Moment coefficients were not measured on the experimental rig, but values of C_m were computed for $\Gamma = -1$, $C_w = 0, 0.06 \le G \le 0.24$, and $1.25 \times 10^6 \le \mathrm{Re}_\phi \le 10^7$. The computed values of C_m for $G = 0.06$ are in close agreement with the computations of Morse (1991a) for $G = 0.1$, and both are close to Dorfman's (1963) widely accepted correlation of C_m for the free disc. The current computations show that C_m decreases as G increases, but this effect is negligible for $G > 0.24$. For $\Gamma = -1$ and $C_w > 0$, the computations show that a superposed flow has only a small effect on C_m: the value of C_m for $\lambda_T = 0.2$ is less than 6 percent larger than that for $\lambda_T = 0$. It appears, therefore, that Dorfman's free-disc correlation should provide a useful estimate of C_m for the designers of cooling systems of gas-turbine engines, where λ_T is usually less than 0.2.

Acknowledgments

The authors wish to thank the Ministry of Defence and the Science and Engineering Research Council (SERC) for supporting the work described in this paper; in particular, the Meiko parallel computer and much of the TSI LDA system was provided by SERC. We also wish to thank the Turkish Government and the University of Uludag, Bursa, for providing financial support for Dr Kilic.

References

Batchelor, G. K. 1951. Note on a class of solutions of the Navier–Stokes equations representing steady rotationally-symmetric flow. *Quart. J. Mech. Appl. Math.*, **4**, 29–41

Cochran, W. G. 1934. The flow due to a rotating disc. *Proc. Camb. Phil. Soc.*, **30**, 365–375

Daily, J. W. and Nece, R. E. 1960. Chamber dimension effects on induced flow and frictional resistance of enclosed rotating disks. *J. Basic Eng., Trans. ASME*, **82**, 217–232

Dijkstra, D. and van Heijst, G. J. F. 1983. The flow between two finite rotating discs enclosed by a cylinder. *J. Fluid Mech.*, **128**, 123–154

Dorfman, L. A. 1963. *Hydrodynamic Resistance and the Heat Loss of Rotating Solids.* Oliver and Boyd, Edinburgh

Gan, X., Kilic, M., and Owen, J. M. 1993. Flow between contra-rotating discs. *ASME International Gas Turbine and Aeroengine Congress* (Paper 93-GT-286), Cincinnati, OH, USA, June 1993. To be published in *J. Turbomachinery*

Graber, D. J., Daniels, W. A., and Johnson, B. V. 1987. Disc pumping test. Wright-Patterson Air Force Base, OH, USA, Report AFWAL-TR-87-2050

Kilic, M. 1993. Flow between contra-rotating discs. Ph.D. thesis, University of Bath, Bath, UK

Kilic, M., Gan, X., and Owen, J. M. 1994. Turbulent flow between two discs contra-rotating at differential speeds. *ASME International Gas Turbine and Aeroengine Congress* (Paper 94-GT-54), Hague, Holland, June 1994. To be published in *J. Turbomachinery*

Launder, B. E. and Sharma, B. I. 1974. Application of the energy dissipation model of turbulence to the calculation of flow near a spinning disc. *Lett. Heat Mass Transfer*, **1**, 131–138

Lonsdale, G. 1988. Solution of a rotating Navier–Stokes problem by a nonlinear multigrid algorithm. *J. Comp. Phys.*, **74**, 177–190

Morse, A. P. 1988. Numerical prediction of turbulent flow in rotating cavities. *J. Turbomachinery*, **110**, 202–215

Morse, A. P. 1991a. Assessment of laminar-turbulent transition in closed disc geometries. *J. Turbomachinery*, **113**, 131–138

Morse, A. P. 1991b. Application of a low Reynolds number k–ε turbulence model to high-speed rotating cavity flows. *J. Turbomachinery*, **113**, 98–105

Nagano, Y. and Hishida, M. 1987. Improved form of the k-ε model for wall turbulent shear flows. *J. Fluid Eng.*, **109**, 156–160

Owen, J. M. and Rogers, R. H. 1989. *Flow and Heat Transfer in Rotating Disc Systems, Vol. 1: Rotor Stator Systems.* Research Studies Press, Taunton (John Wiley Inc., New York)

Patankar, S. V. 1980. *Numerical Heat Transfer and Fluid Flow.* Hemisphere, New York

Stewartson, K. 1953. On the flow between two rotating coaxial disks. *Proc. Camb. Phil. Soc.*, **49**, 333–341

van Doormaal, J. P. and Raithby, G. D. 1984. Enhancements of the SIMPLE method for predicting incompressible fluid flow. *Numer. Heat Transfer*, **7**, 147–163

Vaughan, C. M., Gilham, S., and Chew, J. W. 1989. Numerical solutions of rotating disc flows using a non-linear multigrid algorithm. *Proc. 6th Int. Conf. Numer. Meth. Laminar Turbulent Flow*. Pineridge Press, Swansea, 66–73

Zandbergen, P. J. and Dijkstra, D. 1987. Von Karman swirling flows. *Annu. Rev. Fluid Mech.*, **19**, 465–491

Appendix

The axisymmetric equations for the conservation of mass, momentum, and the turbulence quantities k and ε can be written for incompressible flow in cylindrical-polar coordinates by

$$\frac{1}{r}\frac{\partial}{\partial r}(rV_r) + \frac{\partial V_z}{\partial z} = 0$$

$$\frac{\partial}{\partial r}(\rho r V_r \Phi) + \frac{\partial}{\partial z}(\rho r V_z \Phi) = \frac{\partial}{\partial r}\left(r\Gamma_r \frac{\partial \Phi}{\partial r}\right) + \frac{\partial}{\partial z}\left(r\Gamma_z \frac{\partial \Phi}{\partial z}\right) + S_\Phi$$

where Φ can represent V_r, V_ϕ, V_z, k, or ε, and values of Γ_r, Γ_z, and S_Φ are given in Table A1.

For the LR k–ε turbulence model

$$\mu_{\text{eff}} = \mu + \mu_T$$

$$\mu_T = C_\mu f_\mu \frac{\rho k^2}{\varepsilon}$$

$$P = \mu_T\left[2\left(\left(\frac{\partial V_z}{\partial z}\right)^2 + \left(\frac{\partial V_r}{\partial r}\right)^2 + \left(\frac{V_r}{r}\right)^2\right) + \left(\frac{\partial V_z}{\partial r} + \frac{\partial V_r}{\partial z}\right)^2 + \left(\frac{\partial V_\phi}{\partial z}\right)^2 + \left(r\frac{\partial}{\partial r}\left(\frac{V_\phi}{r}\right)\right)^2\right]$$

Values and expressions for C_μ, f_μ, and other turbulence quantities are given in Table A2.

Table A1 Components of the momentum equations

Φ	Γ_z	Γ_r	S_Φ
V_z	$2\mu_{\text{eff}} - \mu$	μ_{eff}	$-\frac{\partial}{\partial z}\left(p + \frac{2}{3}\rho k\right) + \frac{1}{r}\frac{\partial}{\partial r}\left(r\mu_t \frac{\partial V_r}{\partial z}\right)$
V_r	μ_{eff}	$2\mu_{\text{eff}} - \mu$	$-\frac{\partial}{\partial_r}\left(p + \frac{2}{3}\rho k\right) - (2\mu_{\text{eff}} - \mu)\frac{V_r}{r^2} + \frac{\rho V_\phi^2}{r} + \frac{\partial}{\partial z}\left(\mu_t \frac{\partial V_z}{\partial r}\right)$
V_ϕ	μ_{eff}	μ_{eff}	$-\frac{\rho V_r V_\phi}{r} - \mu_{\text{eff}}\frac{V_\phi}{r^2} - \frac{V_\phi}{r}\frac{\partial \mu_t}{\partial r}$
k	$\mu + \frac{\mu_t}{\sigma_k}$	$\mu + \frac{\mu_t}{\sigma_k}$	$P - \rho\varepsilon - D$
ε	$\mu + \frac{\mu_t}{\sigma_\varepsilon}$	$\mu + \frac{\mu_t}{\sigma_\varepsilon}$	$\frac{\varepsilon}{k}(C_{\varepsilon 1}P - f_1 C_{\varepsilon 2}\rho\varepsilon) + E - F$

Table A2 Terms appearing in the k–ε turbulence models

Term	High R_T model	Launder and Sharma model (LS)	Morse model (M)
C_μ	0.09	0.09	0.09
$C_{\varepsilon 1}$	1.44	1.44	1.44
$C_{\varepsilon 2}$	1.92	1.92	1.92
D	—	$2\mu\left[\left(\frac{\partial\sqrt{k}}{\partial z}\right)^2 + \left(\frac{\partial\sqrt{k}}{\partial r}\right)^2\right]$	$2\mu\left[\left(\frac{\partial\sqrt{k}}{\partial z}\right)^2 + \left(\frac{\partial\sqrt{k}}{\partial r}\right)^2\right]$
E	—	$2\frac{\mu\mu_T}{\rho}\left[\left(\frac{\partial^2 V_r}{\partial z^2}\right)^2 + \left(\frac{\partial^2 V_\phi}{\partial z^2}\right)^2 + \left(\frac{\partial^2 V_z}{\partial r^2}\right)^2 + \left(\frac{\partial^2 V_\phi}{\partial r^2}\right)^2\right]$	$2\frac{\mu\mu_T}{\rho}\left[\left(\frac{\partial^2 V_r}{\partial z^2}\right)^2 + \left(\frac{\partial^2 V_\phi}{\partial z^2}\right)^2 + \left(\frac{\partial^2 V_z}{\partial r^2}\right)^2 + \left(\frac{\partial^2 V_\phi}{\partial r^2}\right)^2\right]$
F	—	—	$2\mu\left[\left(\frac{\partial\sqrt{\varepsilon}}{\partial z}\right)^2 + \left(\frac{\partial\sqrt{\varepsilon}}{\partial r}\right)^2\right]$
f_1	1.0	$(1 - 0.3\exp(-R_T^2))$	$\left(1 - 0.22\exp\left(-\frac{R_T}{6}\right)^2\right)$
f_μ	1.0	$\exp\left[\frac{-3.4}{\left(1 + \frac{R_T}{50}\right)^2}\right]$	$\left(1 - \exp\left(-\frac{y^+}{24.5}\right)\right)^2$
σ_k	1.0	1.0	1.0
σ_ε	1.3	1.3	1.3